GL-TR-89-0267

AD-A223 660

NASA RADIATION BELT MODELS AP-8 AND AE-8

C. E. Jordan

Radex., Inc.
Three Preston Court
Bedford, MA 01730

September 30, 1989
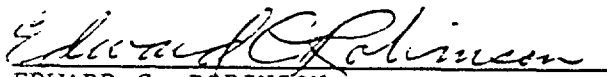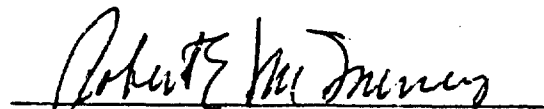
Scientific Report No. 1

Approved for public release; distribution unlimited
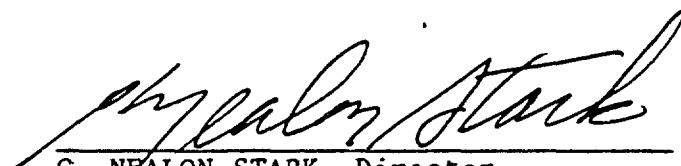
90 06 28 059

"This technical report has been reviewed and is approved for publication"

Edward C. Robinson
EDWARD C. ROBINSON
Contract Manager
Data Systems Branch
Aerospace Engineering Division

Robert E. McInerney
ROBERT E. McINERNEY, Chief
Data Systems Branch
Aerospace Engineering Division

FOR THE COMMANDER

C. Nealon Stark
C. NEALON STARK, Director
Aerospace Engineering Division

This report has been reviewed by the ESD Public Affairs Office (PA) and is releasable to the National Technical Information Service (NTIS).

Qualified requestors may obtain additional copies from the Defense Technical Information Center. All others should apply to the National Technical Information Service.

If your address has changed, or if you wish to be removed from the mailing list, or if the addressee is no longer employed by your organization, please notify GL/IMA, Hanscom AFB, MA 01731. This will assist us in maintaining a current mailing list.

Do not return copies of this report unless contractual obligations or notices on a specific document requires that it be returned.

REPORT DOCUMENTATION PAGE

1a. REPORT SECURITY CLASSIFICATION Unclassified		1b. RESTRICTIVE MARKINGS		
2a. SECURITY CLASSIFICATION AUTHORITY		3. DISTRIBUTION / AVAILABILITY OF REPORT approved for public release; distribution unlimited		
2b. DECLASSIFICATION / DOWNGRADING SCHEDULE				
4. PERFORMING ORGANIZATION REPORT NUMBER(S)		5. MONITORING ORGANIZATION REPORT NUMBER(S) GL-TR-89-0267		
6a. NAME OF PERFORMING ORGANIZATION Radex, Inc.	6b. OFFICE SYMBOL (If applicable)	7a. NAME OF MONITORING ORGANIZATION Geophysics Laboratory		
6c. ADDRESS (City, State, and ZIP Code) Three Preston Court Bedford, MA 01730		7b. ADDRESS (City, State, and ZIP Code) Hanscom AFB Bedford, MA 01731		
8a. NAME OF FUNDING / SPONSORING ORGANIZATION Aerospace Engineering Div	8b. OFFICE SYMBOL (If applicable) LCY	9. PROCUREMENT INSTRUMENT IDENTIFICATION NUMBER Contract F19628-89-C-0068		
8c. ADDRESS (City, State, and ZIP Code)		10. SOURCE OF FUNDING NUMBERS		

8c. ADDRESS (City, State, and ZIP Code)	PROGRAM ELEMENT NO. 62101F	PROJECT NO. 7659	TASK NO. 05	WORK UNIT ACCESSION NO. AB

11. TITLE (include Security Classification)

NASA Radiation Models AP-8 and AE-8

12. PERSONAL AUTHOR(S)

Carolyn E. Jordan

13a. TYPE OF REPORT Scientific No. 1	13b. TIME COVERED FROM 6/89 TO 9/89	14. DATE OF REPORT (Year, Month, Day) 1989 Sep 30	15. PAGE COUNT 26

16. SUPPLEMENTARY NOTATION

17.	COSATI CODES		18. SUBJECT TERMS (Continue on reverse if necessary and identify by block number)
FIELD	GROUP	SUB-GROUP	Radiation belts, trapped particle models, NASA models, AE-8, and AP-8

19. ABSTRACT (Continue on reverse if necessary and identify by block number)

Empirical models AP-8 and AE-8 for the trapped protons and electrons in the Earth's radiation belts are currently available from NSSDC. These are the culmination of a series of models developed by J.I.Vette and colleagues. The initial models were begun in the mid-sixties with the most recent model, AE-8, being released in 1980. These models are based on data ranging from 1958 to 1970. They have been well documented in a variety of sources. No official documentation on AE-8 is available, though a recent report published by TREND, a group working under a contract with ESA, contains some information on this model. The only models which are still available from NSSDC are the most recent proton and electron models AP-8 and AE-8. This document contains a brief summary of the modeling efforts to date based on information from Lemaire, Spjeldvik, and Rothwell. Results from AE8MAX, results from the models previously used at GL (AE6MAX + AEI7HI), and results from code provided by NSSDC are compared.

20. DISTRIBUTION / AVAILABILITY OF ABSTRACT ☒ UNCLASSIFIED/UNLIMITED ☐ SAME AS RPT. ☐ DTIC USERS	21. ABSTRACT SECURITY CLASSIFICATION Unclassified	
22a. NAME OF RESPONSIBLE INDIVIDUAL Edward C. Robinson	22b. TELEPHONE (Include Area Code) (617) 377-3840	22c. OFFICE SYMBOL GL/LCY

DD FORM 1473, 84 MAR

83 APR edition may be used until exhausted.
All other editions are obsolete.

SECURITY CLASSIFICATION OF THIS PAGE

ACKNOWLEDGEMENTS

Accession For		
NTIS GRA&I	⊠	
DTIC TAB	☐	
Unannounced	☐	
Justification		
By		
Distribution/		
Availability Codes		
Dist	Avail and/or Special	
A-1		

TABLE OF CONTENTS

LIST OF FIGURES

LIST OF TABLES

1. INTRODUCTION

Empirical models AP-8 and AE-8 for the trapped protons and electrons in the Earth's radiation belts are currently available from NSSDC [*Bilitza,* 1989]. These are the culmination of a series of models developed by J. I. Vette and colleagues [*NASA/NSSDC Series,* 1966-1976]. The initial models were begun in the mid-sixties with the most recent model, AE-8, being released in 1980. These models are based on data ranging from 1958 to 1970. They have been well documented in a variety of sources [*Lemaire et al.,* 1989; *Spjeldvik and Rothwell,* 1985]. However, no official documentation on AE-8 was ever produced. Recently, Vette has contributed to a report published by TREND, a group working under a contract with ESA, which contains some information on this model [*Lemaire et al.,* 1989].

The only models which are still available from NSSDC are the most recent proton and electron models AP-8 and AE-8. Following is a brief summary of the modelling efforts to date based on information in Lemaire et al. [1989] and Spjeldvik and Rothwell [1985]. Finally, results from AE8MAX compared to results from the models previously used at GL (AE6MAX + AEI7HI) along with results from code provided by NSSDC will be presented.

2. MODELS

2.1 Initial Models : AE-1, -2, and -3, AP-1, -2, -3, and -4

AE-1, AE-2, and AE-3 were the first attempts to model the trapped electrons. AE-1 was an inner belt model (1.2 - 3.0 R_E) for energies of 0.3 - 7.0 MeV. Using B,L coordinates, one could obtain integral omnidirectional flux. The model had a July 1963 epoch (note, the Starfish nuclear explosion was not corrected for). AE-2 was an outer belt model (to 6.3 R_E) for energies of 0.04 - 7.0 MeV. Due to large temporal variations in this region, averages were taken over long intervals (six months or more). Again, Starfish was not taken into account. Despite a clear dependence on local time, this factor was ignored because of large time variations. AE-3 extended AE-2 out to the geosynchronous region (6.6 R_E), even though a geosynchronous satellite had yet to carry radiation particle instruments (they used a sporadic data set from satellites which crossed this region from August 1959 to November 1965). It covers energies ranging from .01 MeV to 6 MeV. In developing this model it was found that the cumulative probability that the flux observed at any random instant would exceed a selected value (J_1), could be approximated by a lognormal distribution whose standard deviation was energy dependent. This allows one to get an idea of the time behavior without any real understanding of the physics.

AP-1, AP-2, AP-3, and AP-4, was essentially one model divided into four energy ranges. The models were numbered in the order in which they were done, not in order of energy range. Thus, AP-1 covers energies from 30 - 50 MeV, AP-2 covers 15 -30 MEV, AP-3 handles energies $\geq$ 50 MeV, and AP-4 is for the 4 - 15 MeV range. Unlike the electrons, there is a definite dependence of the proton spectrum on the magnetic field intensity. In the inner zone, the spectrum hardens with increasing B for particles in the 30 - 50 MeV range. However, the opposite is true for particles above 50 MeV, thus, complicating the proton spectrum. No effort was made to join the models smoothly together at the boundaries.

2.2 Proton Models : AP-5, -6, and -7

AP-5 was produced for protons ranging from 0.1 MeV to 4.0 MeV for $1.2\ R_E \leq L \leq 6.6\ R_E$. An exponential spectrum was used to represent the data. Note, the flux in the outer zone (L = 3.0 -6.6 R_E) is likely to be high because the detectors could not exclude the higher Z particles which are significant when the ring current is enhanced.

AP-6 incorporated new data in the 4 - 30 MeV range for $1.2\ R_E \leq L \leq 4.0\ R_E$. This time a power law was used for the spectral function. Although the new data clearly showed temporal changes, both adiabatic and nonadiabatic, this could not readily be incorporated into the model.

AP-7 was similar to AP-6, but it used an exponential spectral function. The energy range was the same, but L ranged from $1.15\ R_E$ - $3.0\ R_E$. The model was constructed for epoch January 1969 with data taken from 1961 to 1966.

2.3 Electron Models : AE-4, -5, -6, and -7

AE-4 models electrons with energies between .04 MeV and 4.85 MeV. The database was compiled from 23 instruments flown on 11 satellites from 1959 to 1968. Distinct differences in the average flux over this time period led to a division of this model into two epochs, one for solar maximum and the other for solar minimum (1967 and 1964, respectively). This effect is only apparent between $L = 3 - 5\ R_E$. A low altitude cutoff was used which was analytical rather than based on the data due to insufficient data coverage in this region.

The outer belt electron flux is subject to more rapid changes than is seen in the inner belt. These fluxes are coupled to magnetospheric substorm processes, thus time-averaged models were developed. The geomagnetic field is not azimuthally symmetric in the outer zone, so beyond $L = 5\ R_E$, the standard B,L coordinates must be supplemented with LT. Even with this, the time average fluxes were found to vary for a given local time by factors of 10 to 50 over this nine year period.

AE-5 is an inner zone model based on data from December 1964 to December 1967 (epoch October 1967) covering 1.2 - 2.8 R_E for energies 0.04 - 4.0 MeV. One may obtain either omnidirectional or unidirectional flux as a function of E, B, and L. Three time variations were modelled: a) magnetic storms, b) Starfish decay, and c) solar cycle. For electrons with energies below 0.7 MeV, the solar cycle changes were the most significant. Electrons with energies higher than 0.7 MeV at higher L values were most strongly affected by substorms. Note, for energies greater than 0.69 MeV, the data is limited. Starfish was a factor at low L-shells for intermediate energies (~ 1 MeV).

The quiet day solar cycle variation is defined by taking the ratio of the omni-directional flux measured from solar minimum to a standard reference epoch (chosen as October 1967). The average inner belt electron flux is affected by magnetic storms depending on how often they occur, the magnitude of the flux enhancement, and the duration and characteristics of the storm. Increases in the inner belt flux are infrequent, but they are significant and long lasting. Thus, from this database, it was not possible to model a storm effect. However, a correction was made by taking the ratio of the average electron flux from June 1966 to December 1967 divided by the quiet time electron flux (chosen as October 1967). The largest enhancements were found in the $L = 2 - 4\ R_E$ region depending on energy. Disturbances were also seen to peak around 1 MeV, though this may not always be the case.

2

AE-5 Epoch 1975 Projected was obtained from the AE-5 model for solar minimum conditions with Starfish subtracted out. AE-6 was also derived from AE-5, but for solar maximum conditions. Again Starfish was taken out. New data was included to extend the coverage to late 1969.

AEI-7 was a "non-model" according to the TREND report [*Lemaire et al.*, 1989]. It incorporated Vampola's data from OV1-19 into previous work on an interim basis. However, upon further review, the data above 2 MeV was found to be incorrect. Thus, AEI-7 (both HI and LO, solar maximum and minimum, resp.) was pulled from distribution. The valid part of OV1-19 was later put into AE-8.

2.4 Current Proton Model : AP-8

This model is comprised of data from 34 instruments collected from July 1958 to June 1970. Inclusion of the AZUR data allowed a dependence on solar cycle to be determined. The effect is small. Otherwise, it is a static model. Local time variations were not considered because only particles with energy < 10 MeV get to regions beyond $L = 3$ R_E where local time effects are seen. This model includes differential as well as integral flux. The differential results are not as solid as the integral results, plus numerical derivatives are not guaranteed to be smooth. Unidirectional flux is available in addition to the omnidirectional flux. There may be contamination from higher Z particles.

2.5 Current Electron Model : AE-8

This was issued in computer form in 1980, however, no official documentation on it has yet been produced. It is the combination of 3 previous models plus new data:

a) AE-4 (both 1964 and 1967),
b) AE-5 1975 Projected (solar minimum conditions),
c) AE-6 (solar maximum conditions),
d) Vampola's spectrometer OV3-3,
e) Vampola's spectrometer OV1-19,
f) Hovestadts's threshold detector on AZUR (1.5 and 4.5 MeV), and
g) Paulikas and Blake's ATS 6 experiment (highest threshold was 3.9 MeV).

The new data showed that previous results gave a low energy spectrum above 2 MeV. The atmospheric cutoff for this model is strictly empirical. No data set used to obtain AE-4 could give that cutoff directly. The new data from AZUR is suitable for this purpose. A fairly low altitude cutoff was used from this data set which incorporates transient populations (probably due to ring current enhancements).

The local time variation was extended down to 3 R_E by using the AZUR >1.5 MeV data for AE-8 MAX. Finally, this model interfaces the inner and outer zones (this had been done previously, but not released as a separate model and only done roughly). This was done over the $L = 2.4 - 2.8$ R_E region. The inner zone has an energy range of .04 - 4.0 MeV and the outer zone has a range of .04 - 7.0 MeV. The L range is from 1.2 R_E to 11.0 R_E.

The model is in a matrix form with the omnidirectional integral flux a function of energy, B/B_o, and L. The local time dependence was averaged out, since this would occur with a satellite over time in its orbit. Plus, adding a new variable to the matrix would increase its size by a factor of 5. Differential fluxes may be obtained as well as the omnidirectional fluxes (like AP-8). The model is still quasi-static.

3

3. BRIEF DESCRIPTION OF GL SOFTWARE

For the purpose of simulating some of the instruments on CRRES, a package was developed here to simulate the High Energy Electron Spectrometer (HEES). Two models were used to give the electron fluxes in the inner and outer belts, respectively, AE6MAX and AEI7HI. Depending on the L-shell, one or the other model was used. Between 2.6 and 3.4 R_E both were used with an interpolation scheme to obtain the flux. This package will be referred to as HEES.

It was then found that a more recent electon model was available from NSSDC [*Bilitza*, 1989], AE-8: AE8MIN (1986, solar minimum) and AE8MAX (1990, solar maximum). Since CRRES launches in 1990, the model which will be most useful in the instrument simulations is the AE8MAX model. Thus, this was acquired over SPAN from NSSDC. Along with the model itself, two codes were also obtained which use the models. MODEL87 and RADBELT are slightly different versions of the same program which yield the same results. So in comparisons with the HEES code and the modified code (HEES8) which uses AE8MAX rather than the combination of AE6MAX and AEI7HI, only RADBELT was used.

4. RESULTS

4.1 Omnidirectional Results from the Three Codes : HEES, HEES8, and RADBELT

In the subsequent table and plots, it is seen that HEES8 gives accurate results compared to what one obtains from RADBELT. One also sees that the results are reasonable although somewhat different from those obtained using the combination of the two older models. First the omnidirectional integral fluxes were compared. Integral flux (electrons $cm^{-2} s^{-1}$) takes into account all of the flux above a given energy threshold.

Table 1 gives the logarithm of the equatorial electron integral fluxes for each of 10 sample energy channels at 19 L-shells. None of the models give results for L = 1 R_E, nor have any information for energies of 8 MeV or higher. The zeros seen in this table show the limits of the models in terms of L-shell and energy. HEES8 and RADBELT show excellent agreement throughout the range of data generated. This simply confirms the correct incorporation of the new model into the in-house software. For the lower L-shells ($\leq 2 R_E$), HEES and HEES8 match exactly. This again indicates proper incorporation of AE8MAX in HEES8. However, beyond this, differences arise. This may be attributed both to model differences and to differences in handling the interpolation between the inner and outer belts. At lower L values, HEES gives lower fluxes than HEES8, except at the highest energies (4 and 6 MeV). By L = 3.5 R_E, only the lowest energy channel (0.5 MeV) is smaller according to HEES, the rest are all greater than HEES8. As one goes to L = 7 R_E, even this energy channel is larger when given by HEES rather than by HEES8. At L = 7 R_E though, HEES8 gives larger results for the higher energies (≥ 2 MeV) than HEES. For L = 8 and 8.5 R_E, all energies from HEES8 show higher fluxes and more energy channels give results than from HEES. For L = 9 - 10 R_E, the lowest energy channel is again higher for HEES, but HEES8 is larger for the rest and still goes to higher energies than does HEES. This is in agreement with a brief note from NSSDC which points out three differences of AE-8 from its predecessors (and basis models) AE-4, AE-5, and AE-6. AE-7 is not mentioned, but on the basis of the TREND report [*Lemaire et al.*, 1989], one may conclude that the differences seen in the outer zone for particles above 2 MeV are attributable to the different usage of the OV1-19 data in AEI7HI and AE8MAX. There were no modifications to AE-5 and AE-6. Hence, the agreement at low L-shells.

Table 1: Flux Found from Models AE8MAX and AE6MAX + AEI7LO using modified HEES8 and HEES code and RADBELT (from NSSDC). Note, $B/B_o = 1$.

L-Shell	Energy (MeV)	LOG (Model Fluxes)		
		HEES	HEES8	RADBELT
1.0	0.5	0.	0.	0.
	1.0	0.	0.	0.
	1.5	0.	0.	0.
	2.0	0.	0.	0.
	2.5	0.	0.	0.
	3.0	0.	0.	0.
	3.5	0.	0.	0.
	4.0	0.	0.	0.
	6.0	0.	0.	0.
	8.0	0.	0.	0.
1.5	0.5	6.740234	6.740234	6.740205
	1.0	5.934570	5.934570	5.934549
	1.5	5.556641	5.556641	5.556664
	2.0	5.230469	5.230469	5.230449
	2.5	4.902344	4.902344	4.902329
	3.0	4.041016	4.041016	4.040998
	3.5	2.955078	2.955078	2.955062
	4.0	1.869141	1.869141	1.869114
	6.0	0.	0.	0.
	8.0	0.	0.	0.
2.0	0.5	6.886719	6.886719	6.886716
	1.0	4.892578	4.892578	4.892595
	1.5	4.129883	4.129883	4.130012
	2.0	3.504883	3.504883	3.504878
	2.5	2.886719	2.886719	2.886716
	3.0	2.037109	2.037109	2.037028
	3.5	1.319336	1.319336	1.319314
	4.0	0.601563	0.601563	0.601517
	6.0	0.	0.	0.
	8.0	0.	0.	0.
2.5	0.5	6.477879	6.524414	6.524396
	1.0	4.768419	4.999023	4.999043
	1.5	3.977416	4.601563	4.601517
	2.0	3.219738	4.029297	4.029384
	2.5	2.534250	3.332031	3.332034
	3.0	1.423225	2.498047	2.498035
	3.5	0.592728	1.511719	1.511750
	4.0	0.560872	0.446289	0.446226
	6.0	0.367886	0.	0.
	8.0	0.	0.	0.

5

Table 1. (Cont'd)

L-Shell	Energy (MeV)	LOG (Model Fluxes)		
		HEES	HEES8	RADBELT
3.0	0.5	6.427165	6.476563	6.476542
	1.0	5.672363	6.033203	6.033021
	1.5	5.247632	5.698242	5.698275
	2.0	4.832422	5.341797	5.341830
	2.5	4.503675	4.991211	4.991226
	3.0	4.053346	4.632813	4.632862
	3.5	3.697243	4.254883	4.254790
	4.0	3.506107	3.885742	3.885757
	6.0	2.348192	2.300563	2.300595
	8.0	0.	0.	0.
3.5	0.5	6.654548	6.770508	6.770484
	1.0	6.344085	6.332031	6.332034
	1.5	6.115120	6.020508	6.020361
	2.0	5.886156	5.723633	5.723620
	2.5	5.691566	5.406250	5.406199
	3.0	5.496975	5.079102	5.079181
	3.5	5.268515	4.698242	4.698275
	4.0	5.040055	4.242188	4.242293
	6.0	3.496975	1.747820	1.747800
	8.0	0.	0.	0.
4.0	0.5	6.954102	6.958984	6.958994
	1.0	6.652344	6.504883	6.504878
	1.5	6.436035	6.204102	6.204120
	2.0	6.219727	5.837891	5.837904
	2.5	6.009277	5.498047	5.498035
	3.0	5.798828	5.029297	5.029384
	3.5	5.671387	4.601563	4.601517
	4.0	5.543945	4.060547	4.060698
	6.0	3.762695	1.020189	1.020361
	8.0	0.	0.	0.
4.5	0.5	7.041016	7.044922	7.044932
	1.0	6.723633	6.579102	6.579097
	1.5	6.410156	6.145508	6.145507
	2.0	6.096680	5.715820	5.715836
	2.5	5.857422	5.300781	5.300813
	3.0	5.618164	4.875000	4.875003
	3.5	5.439941	4.397461	4.397419
	4.0	5.261719	3 850586	3.850585
	6.0	3.558594	0.160739	0.160769
	8.0	0.	0.	0.
5.0	0.5	6.954102	7.020508	7.020361
	1.0	6.588867	6.446289	6.446226
	1.5	6.200684	5.954102	5.954098
	2.0	5.812500	5.517578	5.517592
	2.5	5.537598	5.079102	5.079181
	3.0	5.262695	4.623047	4.623042
	3.5	5.053711	4.161133	4.161068
	4.0	4.844727	3.612305	3.612254
	6.0	3.219727	0.	0.
	8.0	0.	0.	0.

Table 1. (Cont'd)

L-Shell	Energy (MeV)	LOG (Model Fluxes)		
		HEES	HEES8	RADBELT
5.5	0.5	6.897461	6.891602	6.891593
	1.0	6.397461	6.242188	6.242293
	1.5	5.954590	5.731445	5.731428
	2.0	5.511719	5.266602	5.266702
	2.5	5.162109	4.805664	4.805637
	3.0	4.812500	4.361328	4.361350
	3.5	4.604980	3.875000	3.875003
	4.0	4.397461	3.332031	3.332034
	6.0	2.758789	0.	0.
	8.0	0.	0.	0.
6.0	0.5	6.762695	6.723633	6.723620
	1.0	6.198242	5.999023	5.999043
	1.5	5.687012	5.454102	5.454082
	2.0	5.175781	4.995117	4.995108
	2.5	4.728516	4.476563	4.476542
	3.0	4.281250	4.044922	4.044932
	3.5	4.062988	3.555664	3.555699
	4.0	3.844727	3.020508	3.020361
	6.0	2.219727	0.	0.
	8.0	0.	0.	0.
6.5	0.5	6.558269	6.505361	6.505421
	1.0	5.903412	5.733513	5.733518
	1.5	5.295669	5.141353	5.141450
	2.0	4.687927	4.666894	4.666892
	2.5	4.149036	4.096215	4.096215
	3.0	3.610144	3.646657	3.646698
	3.5	3.356047	3.250246	3.250176
	4.0	3.101950	2.705316	2.705350
	6.0	1.326277	0.	0.
	8.0	0.	0.	0.
7.0	0.5	6.341797	6.266602	6.266702
	1.0	5.573242	5.414063	5.414137
	1.5	4.888672	4.770508	4.770484
	2.0	4.204102	4.229492	4.229426
	2.5	3.539551	3.601563	3.601517
	3.0	2.875000	3.189453	3.189490
	3.5	2.525391	2.805664	2.805637
	4.0	2.175781	2.370117	2.370143
	6.0	0.	0.	0.
	8.0	0.	0.	0.
7.5	0.5	5.972656	5.928711	5.928703
	1.0	5.041016	4.999023	4.999043
	1.5	4.315918	4.289063	4.289143
	2.0	3.590820	3.662109	3.662096
	2.5	2.795410	3.052734	3.052694
	3.0	2.000000	2.689453	2.689486
	3.5	1.451172	2.341797	2.341830
	4.0	0.902344	2.000000	2.000000
	6.0	0.	0.	0.
	8.0	0.	0.	0.

| Table 1. (Cont'd) | | LOG (Model Fluxes) | | |
L-Shell	Energy (MeV)	HEES	HEES8	RADBELT
8.0	0.5	5.430664	5.498047	5.498035
	1.0	4.397461	4.461914	4.461948
	1.5	3.638672	3.642578	3.642563
	2.0	2.879883	2.977539	2.977541
	2.5	1.939941	2.469727	2.469675
	3.0	1.000000	2.145508	2.145507
	3.5	0.060059	1.844727	1.844726
	4.0	0.	1.590820	1.590842
	6.0	0.	0.	0.
	8.0	0.	0.	0.
8.5	0.5	4.842773	4.843750	4.843731
	1.0	3.499512	3.668457	3.668479
	1.5	2.160468	2.810059	2.810031
	2.0	0.821423	2.187500	2.187521
	2.5	0.	1.765137	1.765147
	3.0	0.	1.488770	1.488833
	3.5	0.	1.243652	1.243534
	4.0	0.	1.006836	1.006894
	6.0	0.	0.	0.
	8.0	0.	0.	0.
9.0	0.5	4.254883	4.189453	4.189490
	1.0	2.601563	2.875000	2.875003
	1.5	0.948242	1.977539	1.977541
	2.0	0.	1.397461	1.397419
	2.5	0.	1.060547	1.060698
	3.0	0.	0.832031	0.832062
	3.5	0.	0.642578	0.642563
	4.0	0.	0.422852	0.422918
	6.0	0.	0.	0.
	8.0	0.	0.	0.
9.5	0.5	3.438965	3.137695	3.137671
	1.0	0.431872	1.786621	1.786609
	1.5	0.	0.988770	0.988782
	2.0	0.	0.698730	0.698709
	2.5	0.	0.530273	0.530328
	3.0	0.	0.416016	0.415974
	3.5	0.	0.321289	0.321391
	4.0	0.	0.211426	0.211388
	6.0	0.	0.	0.
	8.0	0.	0.	0.
10.0	0.5	2.623047	2.085938	2.086004
	1.0	0.	0.698242	0.698275
	1.5	0.	0.	0.
	2.0	0.	0.	0.
	2.5	0.	0.	0.
	3.0	0.	0.	0.
	3.5	0.	0.	0.
	4.0	0.	0.	0.
	6.0	0.	0.	0.
	8.0	0.	0.	0.

Four plots are also given to illustrate the differences seen between HEES and HEES8. Note, that HEES8 and RADBELT agree so well that the two lines (short dash for HEES8 and long dash for RADBELT) overplot each other and show up as only one line in the plots.

Figure 1 shows two plots taken from the Handbook of Geophysics and the Space Environment [*Spjeldvik and Rothwell*, 1985] in the top panels. These show the equatorial omnidirectional integral flux versus energy for the AEI-7 LO and HI models at L = 4.0 R_E (upper left) and at L = 6.6 R_E (upper right). The lower plots were generated from the results given by HEES (AE6MAX + AEI7HI), HEES8 (AE8MAX), and RADBELT (AE8MAX) for L = 4.0 R_E (lower left) and L = 6.5 R_E (lower right). HEES follows the AE7-HI model closely at L = 4.0 R_E, whereas HEES8 and RADBELT follow the AE7-LO model. At L = 6.5 R_E, All three codes give similar results to AE7-HI (at L = 6.6 R_E) with HEES yielding a slightly higher flux than the other two.

Figure 2a shows four plots taken from the Handbook of Geophysics and the Space Environment [*Spjeldvik and Rothwell*, 1985]. Again, equatorial omnidirectional integral fluxes are shown, but this time as a function of L-shell. The results for various energies from AE-6 are shown in the upper left, AE-4 (1967, solar maximum) in the upper right, AE7-LO in the lower left, AE7-HI in the lower right. Similar plots were then made based on the results from HEES, HEES8, and RADBELT. However, for clarity, the various energies were separated into different plots. Thus, Figure 2b shows 0.5 MeV results in the upper left, 1.0 MeV in the upper right, 2.0 Mev in the lower left, and 3.0 MeV in the lower right. Finally, Figure 2c shows 4.0 Mev on the left and 6.0 MeV on the right.

Comparisons of Figures 2b and 2c with 2a show good agreement between the current results with those given in the Handbook [*Spjeldvik and Rothwell*, 1985]. The inner zone results from AE6MAX and AE8MAX agree very well as is predicted in the note from NSSDC [*Bilitza*, 1989]. The outer zone differences are anticipated, however, Bilitza [1989] indicates that for particles above 2MeV, the outer zone flux should be harder. This appears to be the case in comparison with AE-4 (Figure 2a), however, AE8MAX does not peak at as high a flux as AEI7HI. Again this may be credited to the different use of the high energy OV1-19 data in these two models.

4.2 Differential Results from the Two Codes : HEES and HEES8

In additio.1 to the omnidirectional integral flux found from the models, one is also interested in the pitch angle dependent differential flux. Differential flux (electrons cm^{-2} s^{-1} sr^{-1} MeV^{-1}) is the flux obtained from electrons in a given energy range. This is a unidirectional flux rather than an omnidirectional flux, thus, it is per steradian. Figures 3, 4, and 5 are provided to show the differences between current calculations and earlier work [*Spjeldvik and Rothwell*, 1985]. The pitch angle dependent differential flux results are highly dependent on L-shell and energy. Thus, to get a comparison with a plot published in Spjeldvik and Rothwell [1985], the energy range of 575 keV - 775 keV was used to find the flux for L = 1.4 R_E (Figure 3). Then, to examine the flux at different L-shells, several plots were made using the first energy channel of the HEES instrument, 1.0 - 1.5 MeV (Figure 4). Finally, to show changes due to other energy intervals, some plots of flux versus pitch angle for electrons in the 3.5 - 4.0 MeV range were made (Figure 5).

The left side of Figure 3 shows a plot taken from the Handbook of Geophysics and the Space Environment [*Spjeldvik and Rothwell*, 1985]. Here, the AE5 inner belt model is shown along with the Starfish contribution to the electron flux. The plot on the right shows the results from HEES (AE6MAX + AEI7HI) and HEES8 (AE8MAX). Note, HEES and HEES8 yield the same results at L = 1.4 R_E as is expected (the inner belt was not modified from AE6 to AE8).

9

These results agree well with those from AE5. The slightly lower flux is attributable to the decay of the Starfish contribution.

Figure 4a shows the differences between HEES and HEES8 for L = 1.5 - 3.0 R_E. The results are the same for the inner belt. However, some discrepancies arise as one gets into the trough between the two belts. Note, the worst agreement found between these models is seen at L = 2.5 R_E. Here, the fluxes are quite low and uncertain. Thus, one expects the differences to be higher. As the outer belt is approached, HEES8 gives higher fluxes. However, this changes as the peak of the outer belt is reached (Figure 4b).

Figure 4b shows the peak of the outer belt, L = 4.0 - 5.5 R_E. HEES and HEES8 agree well with the best correlation seen at smaller pitch angles. At higher pitch angles, HEES gives slightly higher fluxes than HEES8. HEES continues to give higher fluxes than HEES8 as one goes beyond the outer belt (Figure 4c), until around 8 R_E where HEES8 begins to give larger fluxes. Note, that at this distance, the flux is quite low and is uncertain. Still, for this energy channel, the agreement between the two is quite good. Again, AEI7HI gives slightly higher fluxes at the peak of the outer belt than AE8MAX.

Figure 5 shows the differential flux versus pitch angle for electrons between 3.5 and 4.0 MeV. As with the lower energy particles, the inner belt flux is the same, AE8MAX gives higher fluxes as the outer belt is approached, AEI7HI gives higher fluxes at the peak of the outer belt, and AE8MAX again yields higher fluxes beyond this peak. The relationship between these two models is the same at both energies, however, at the higher energy, the differences are greater. Note, this relationship is the same because the code in use at GL scales the flux from the various high energy channels to the output from the 1 MeV channel. This figure is provided to give the reader an idea of the order of magnitude of the flux at this energy range.

5. SUMMARY

From these comparisons, it is clear that there are significant differences between the outer zone of AE-8 MAX and AEI7HI. In light of the remarks in the TREND report [*Lemaire et al.*, 1989], it is recommended that use of the AEI-7 models be discontinued. These results also indicate that current GL software is producing reasonable results. Hence, it is believed that we may rely on these models for further instrument and data analysis as much as any current static radiation belt models may be relied upon.

10
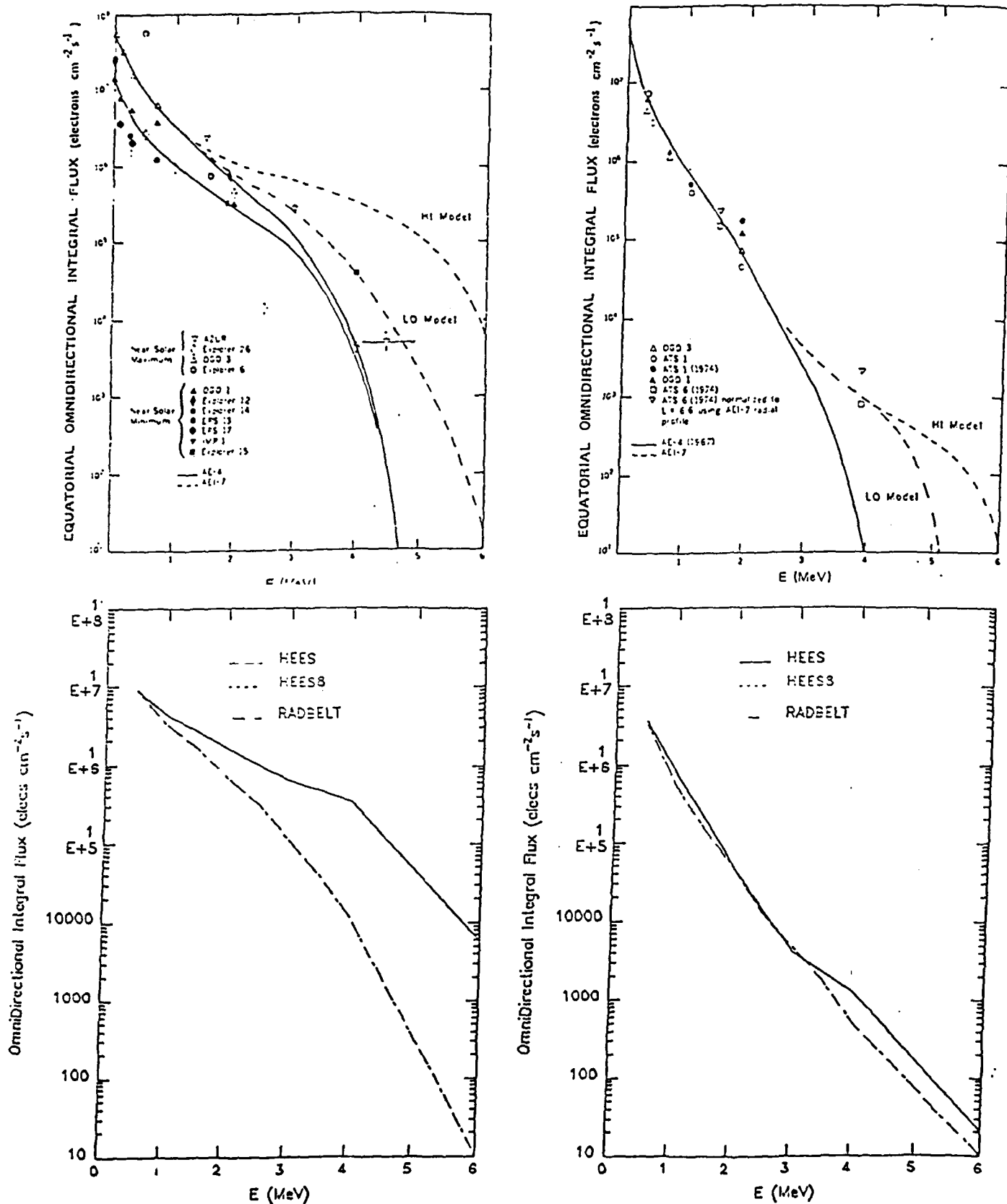
Figure 1: Equatorial Omnidirectional Integral Flux vs. Energy for the AEI-7 LO and HI models at L=4 (upper left) and L=6.6 (upper right) taken from the Handbook of Geophysics and the *Space Environment [Spjeldvik and Rothwell, 1985].* *Lower plots show the results from HEES (AE6MAX + AEI7LO), HEES8 (AE8MAX), and RADBELT (AE8MAX) for L=4 (lower left) and L=6.5 (lower right).* Note, the results from HEES8 and RADBELT are superposed.
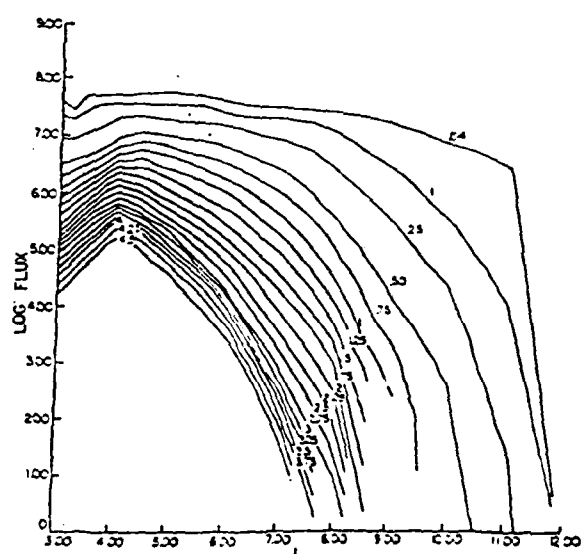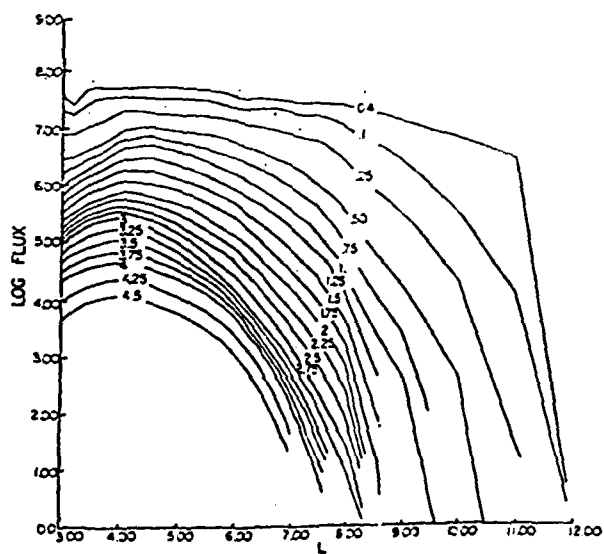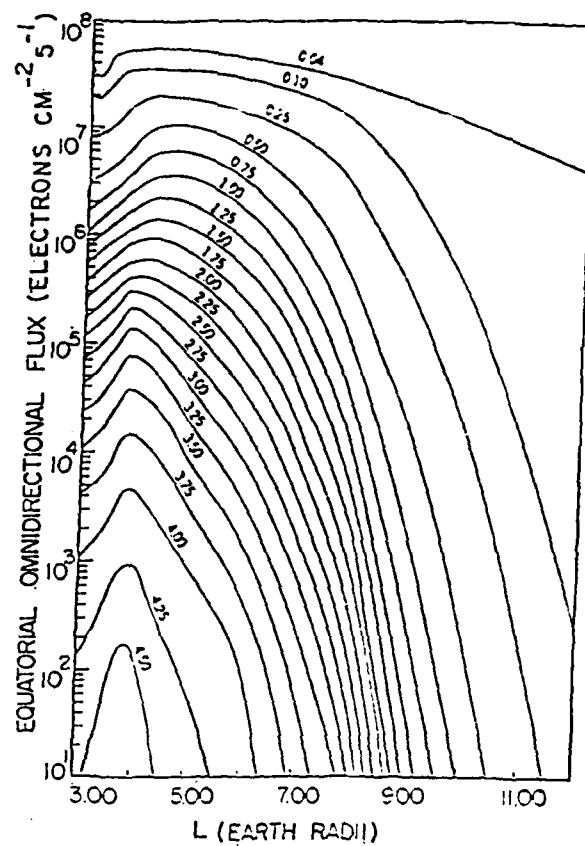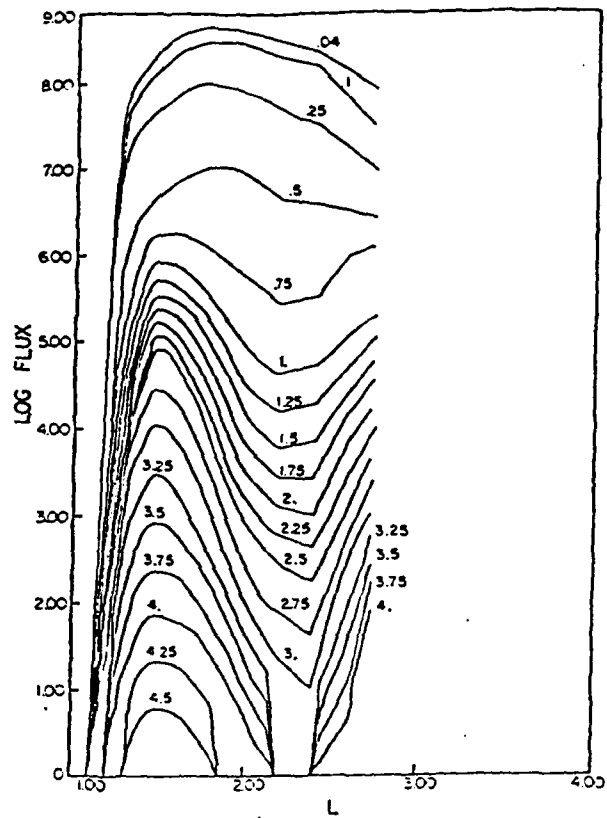
Figure 2a.: Equatorial Omnidirectional Integral Flux vs. L-shell for various energies for AE-6 (upper left), AE-4 (1967, solar maximum, upper right), AE7-LO (lower left), and AE7-HI (lower right).
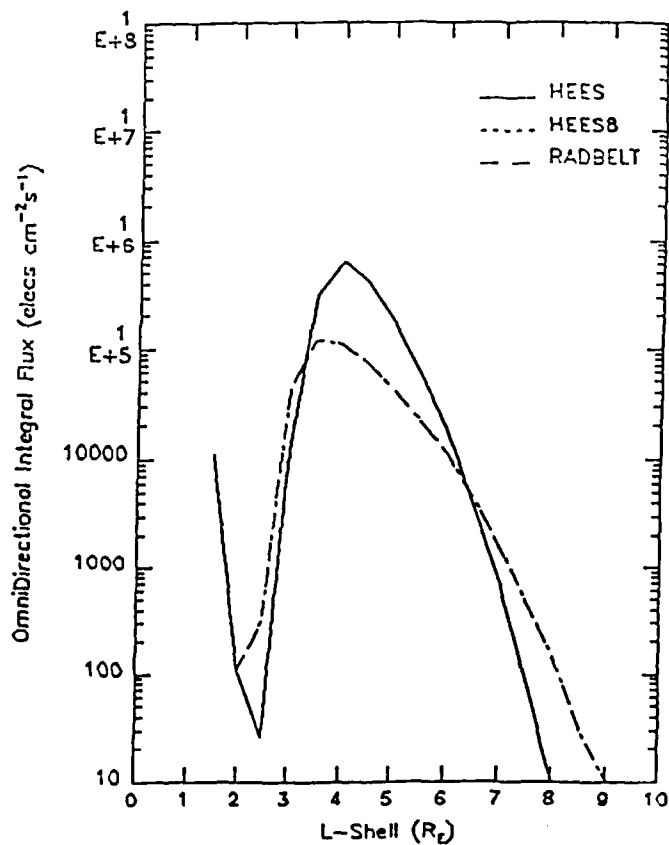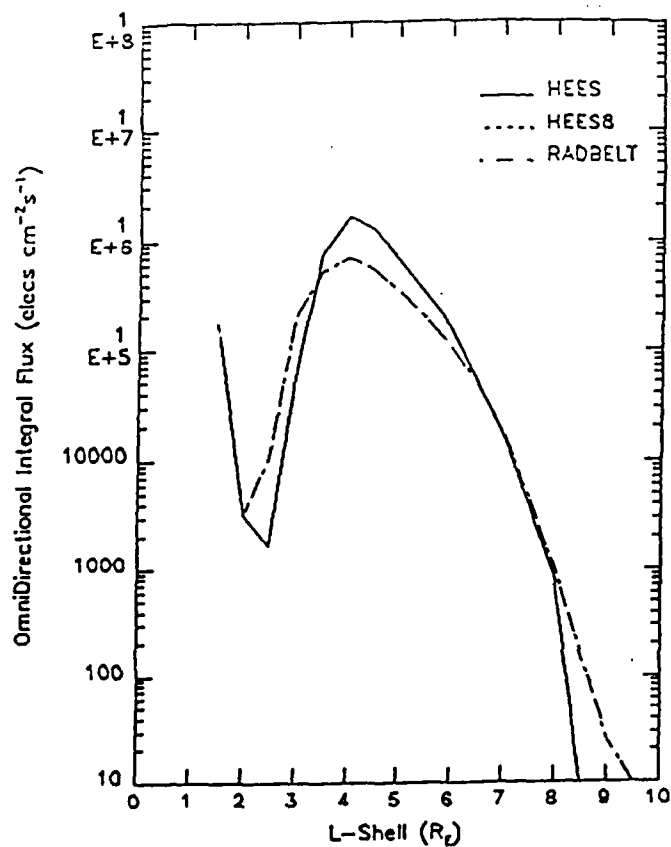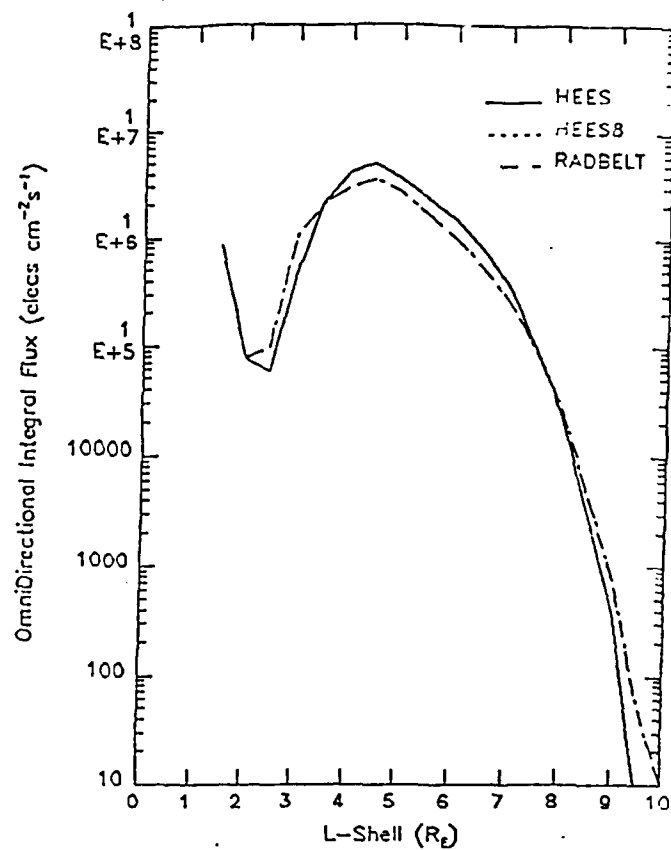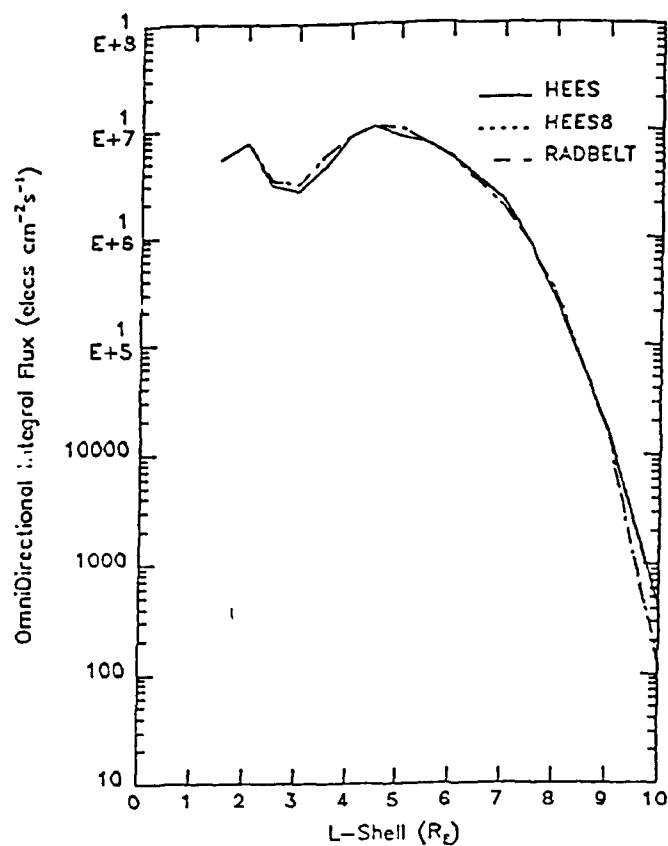
Figure 2b.: Equatorial Omnidirectional Integral Flux vs. L-shell for HEES (AE6MAX + AEI7LO), HEES 8 (AE8MAX), and RADBELT (AE8MAX) for energies of 0.5 MeV (upper left), 1.0 MeV (upper right), 2.0 MeV (lower left, and 3.0 MeV (lower right). Note, the results from HEES8 and RADBELT are superposed.
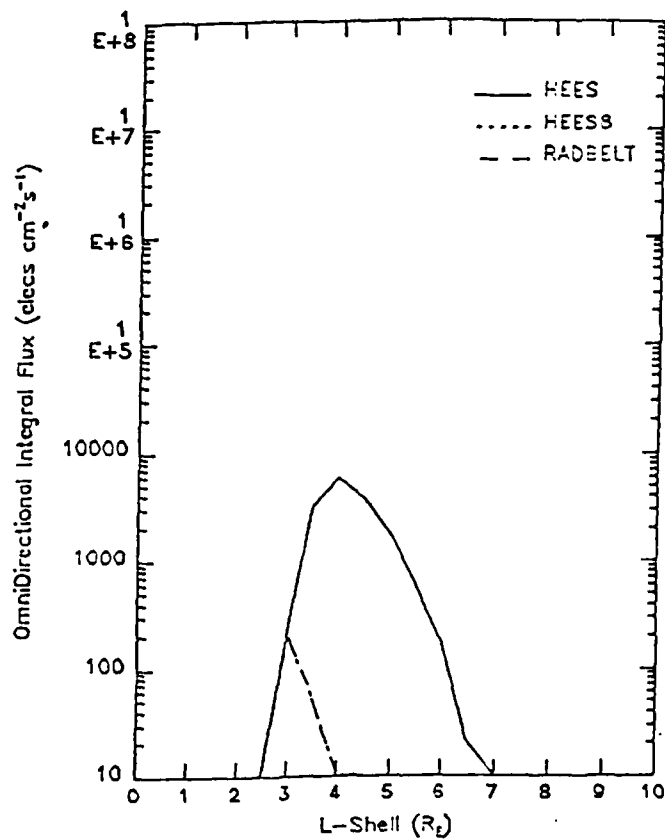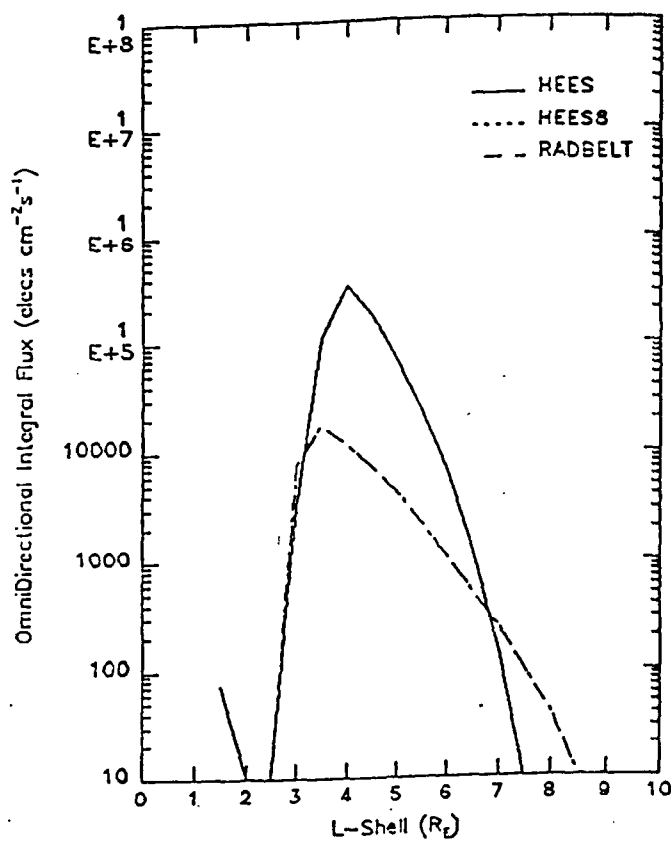
Figure 2c: Equatorial Omnidirectional Integral Flux vs. L-shell for HEES (AE6MAX + AEI7LO), HEES 8 (AE8MAX), and RADBELT (AE8MAX) for energies of 4.0 MeV (left) and 6.0 MeV (right). Note, the results from HEES8 and RADBELT are superposed.
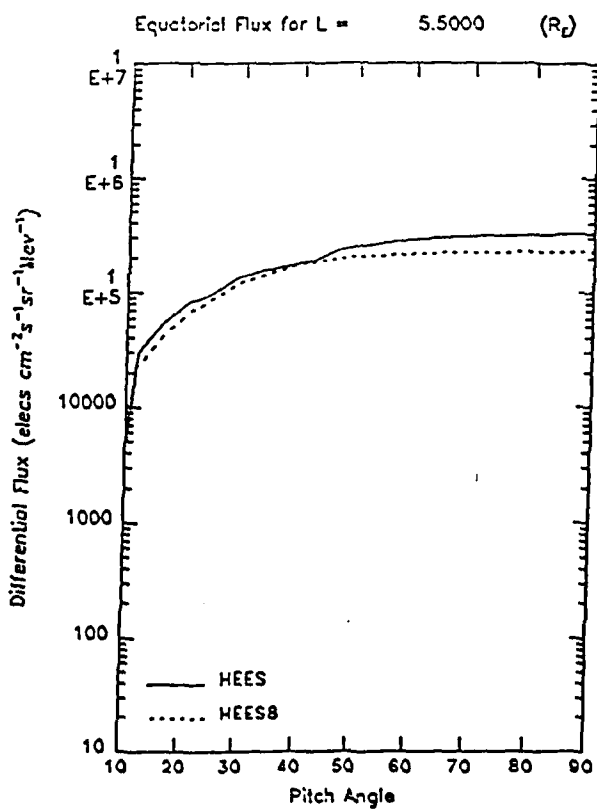
14
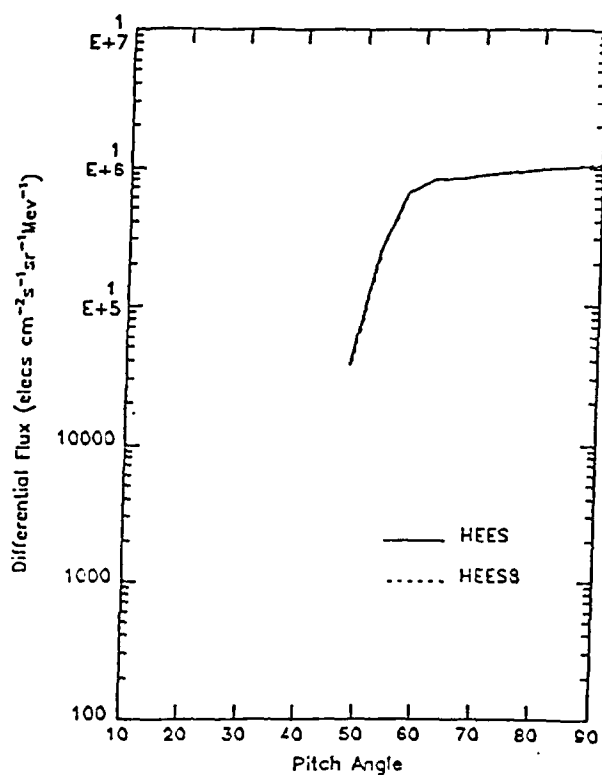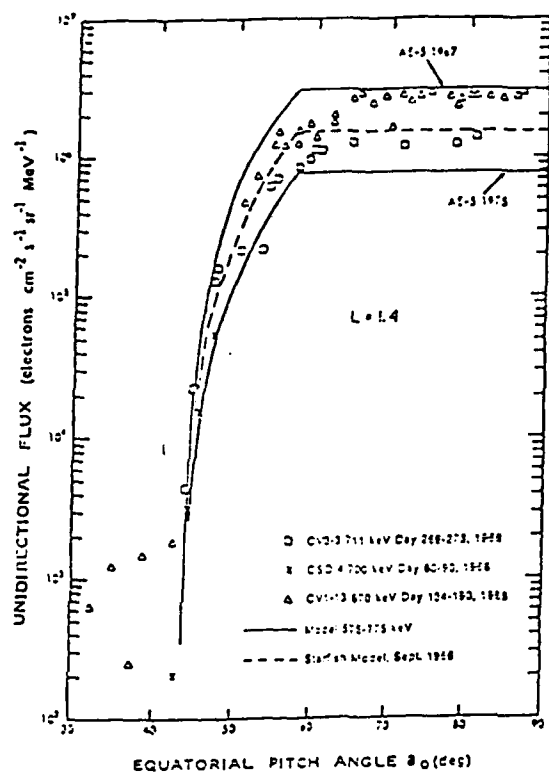
Figure 3: Unidirectional differential flux vs. pitch angle for electrons with energies between 575-775 keV at L=1.4 R_E. Note, the results for HEES (AE6MAX + AEI7HI) and HEES8 (AE8MAX) are superposed. The plot on the right agrees well with the AE-5 1967 (solar maximum) plot on the left, when the Starfish correction is taken into account.
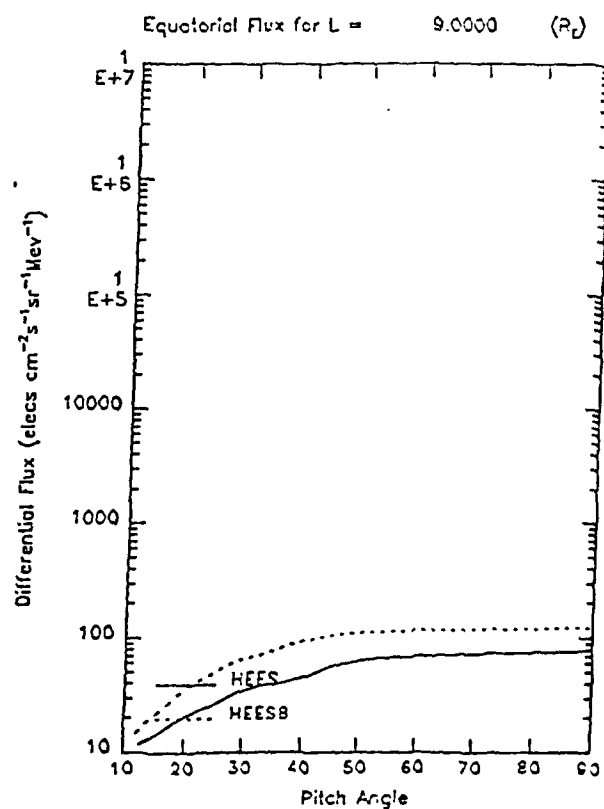
15
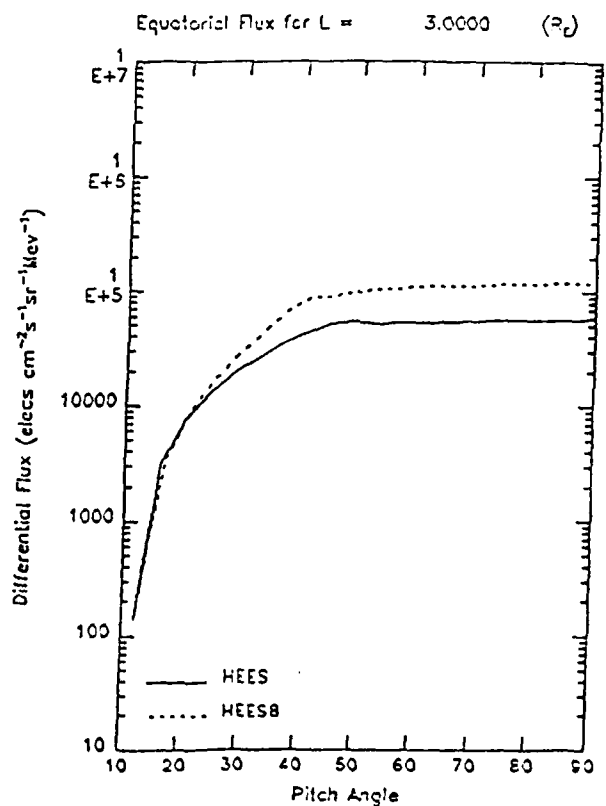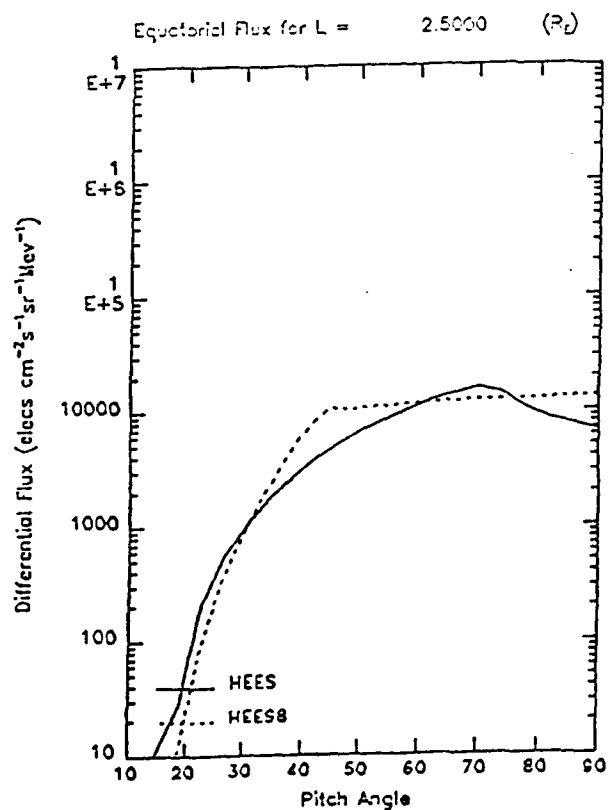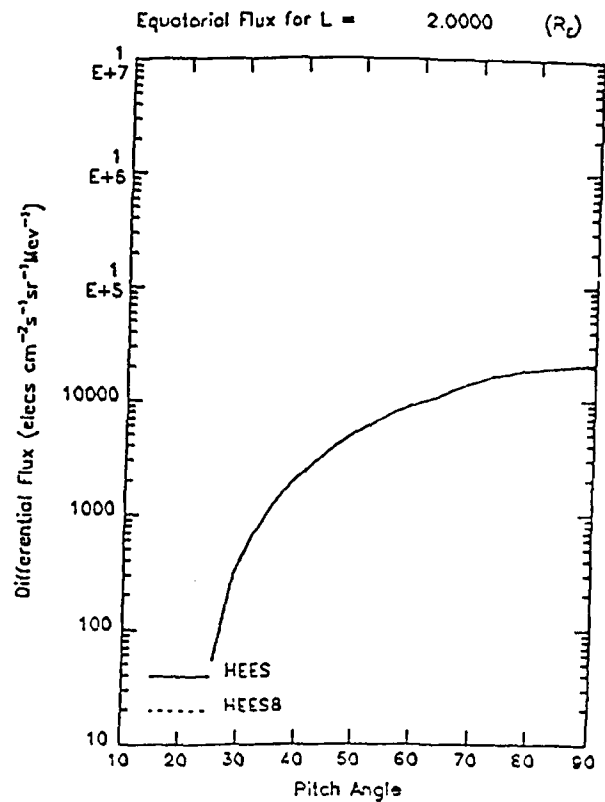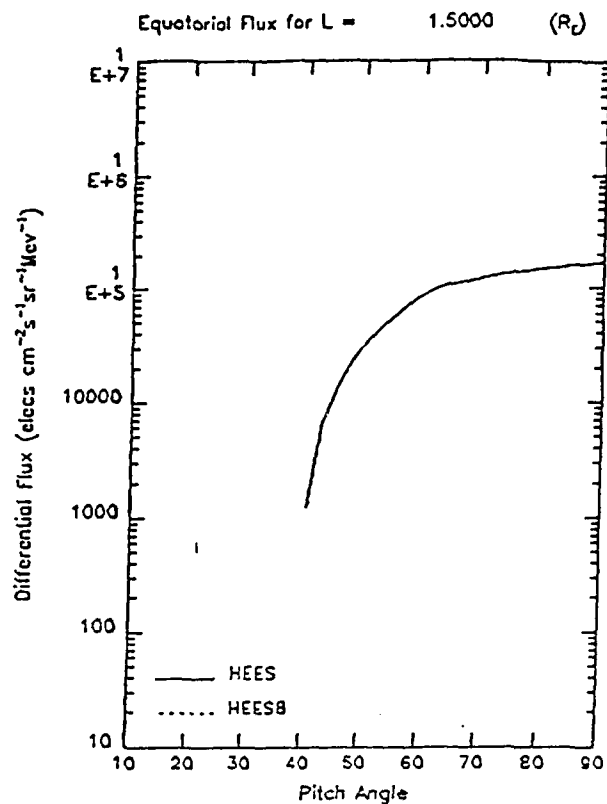
Figure 4a: Unidirectional differential flux vs. pitch angle for electrons with energies between 1.0-1.5 MeV for L=1.5-3.0 R_E. The inner belts agree closely, hence HEES (AE6MAX + AEI7HI) and HEES8 (AE8MAX) are superposed. However, discrepancies arise in the outer zone.

16
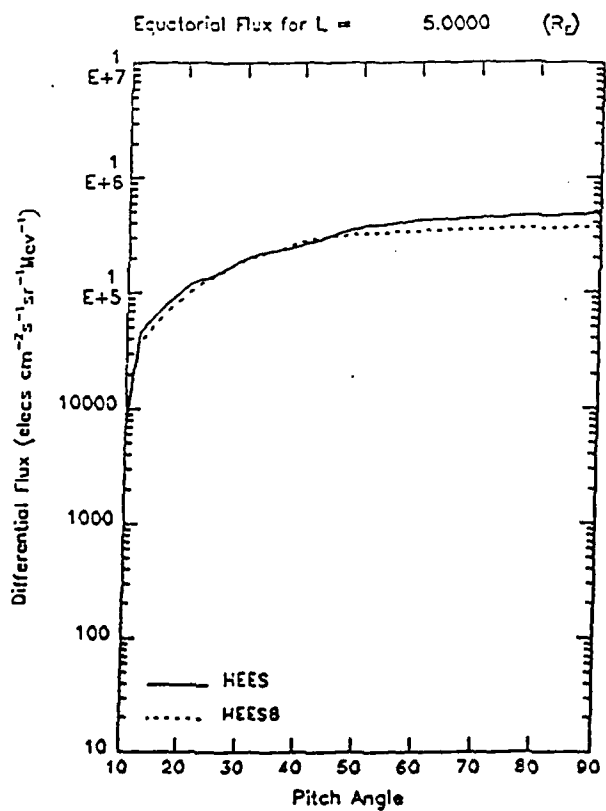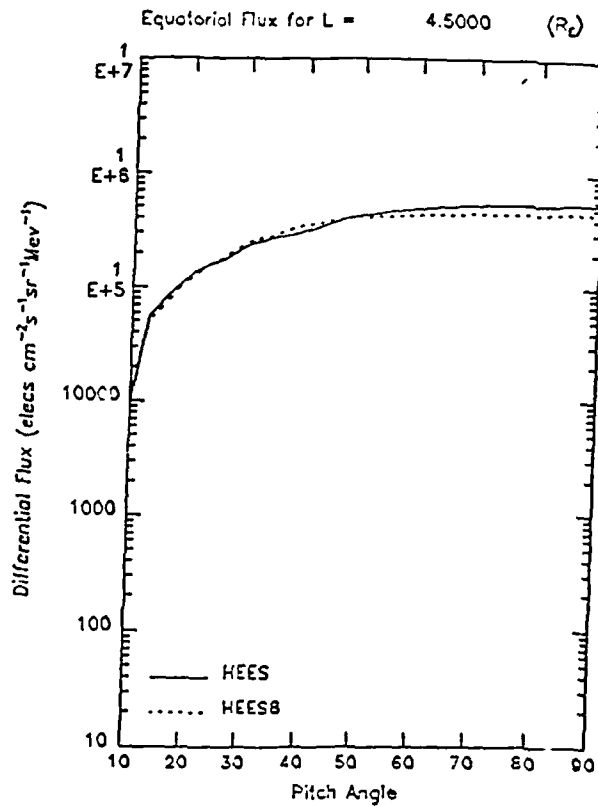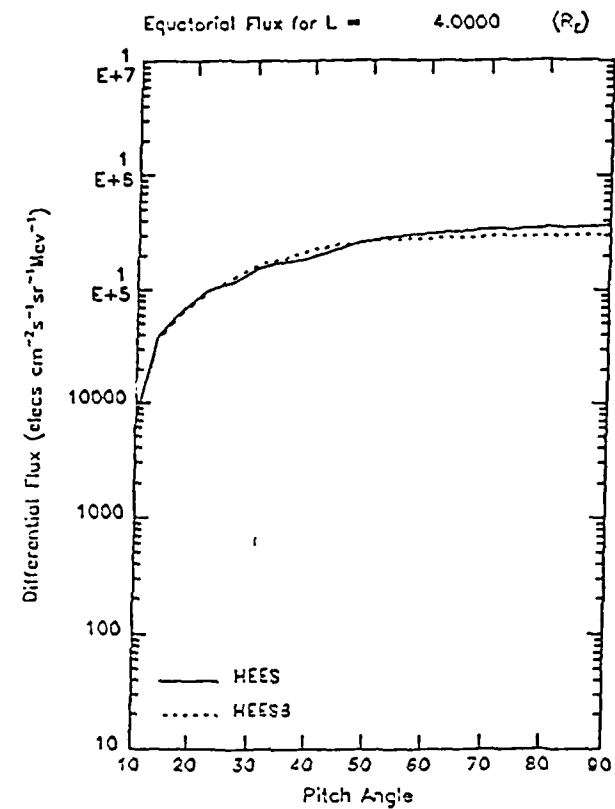
Figure 4b: Unidirectional differential flux vs. pitch angle for electrons with energies between 1.0-1.5 MeV for L=4.0-5.5 R_E. There are small differences between HEES (AE6MAX + AEI7HI) and HEES8 (AE8MAX).
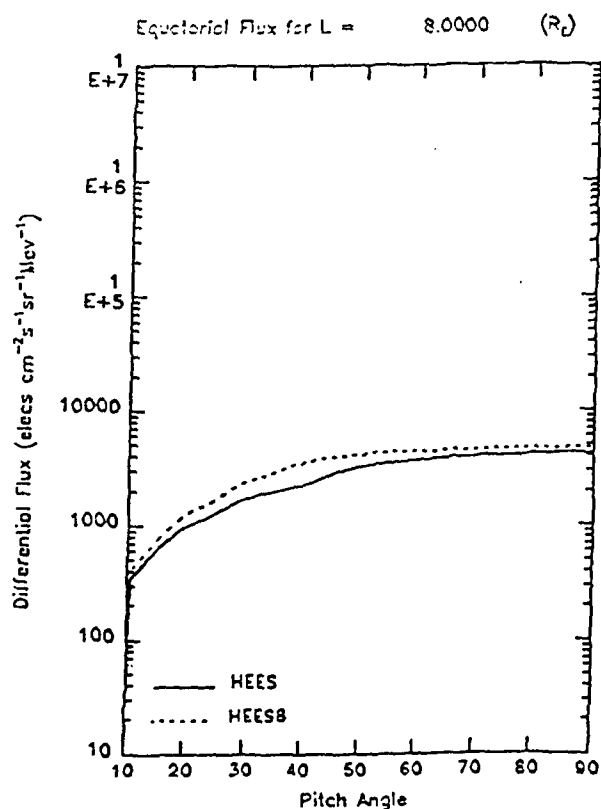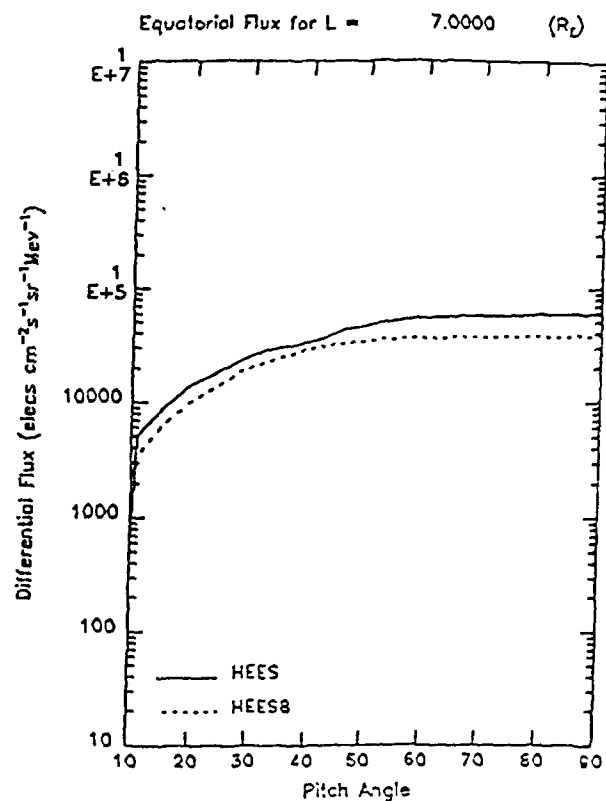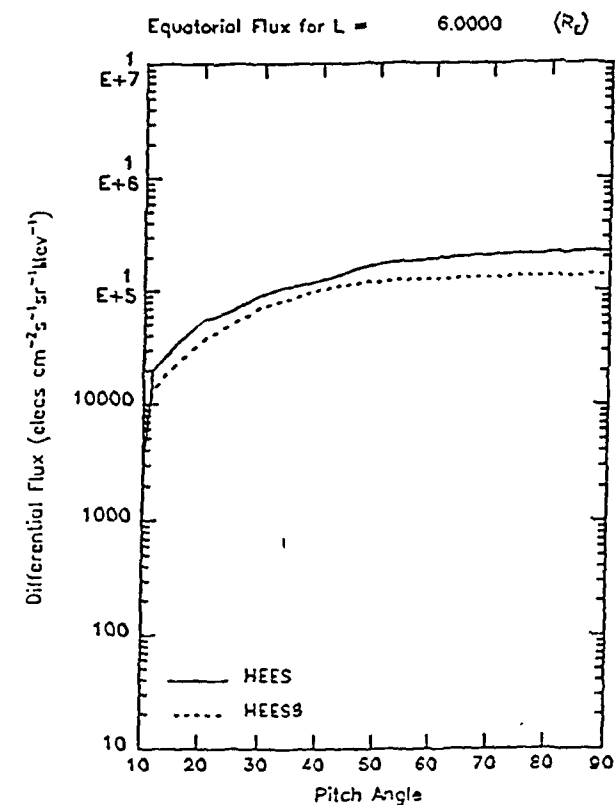
17

Figure 4c: Unidirectional differential flux vs. pitch angle for electrons with energies between 1.0-1.5 MeV for L=6.0-9.0 R_E. The differences are slightly larger than those seen at lower L-shells between HEES (AE6MAX + AEI7HI) and HEES8 (AE8MAX)
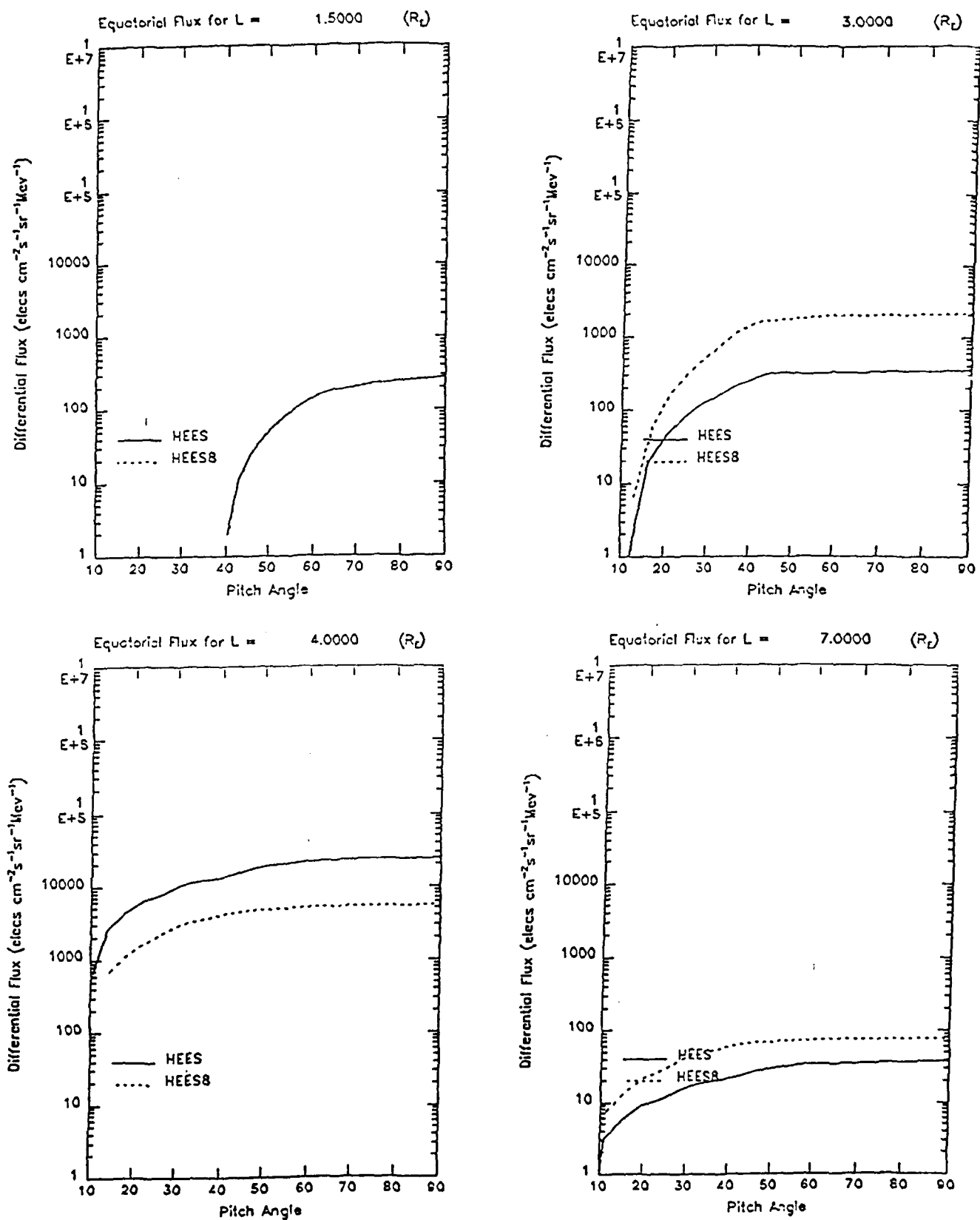
18

Figure 5: Unidirectional differential flux vs. pitch angle for electrons with energies between 3.5-4.0 MeV for L=1.5, 3.0, 4.0, and 7.0 R_E. The same relationship is seen between HEES (AE6MAX + AEI7HI) and HEES8 (AE8MAX) as with the lower energy particles depicted in Figure 4. However, the differences are larger.

19

References

Bilitza, D., various notes and code from his account at NSSDC (NSSDCA::NCF_ACQ_USER:[BILITZA.TRM]) via the SPAN network, obtained July 1989.

Lemaire, J., Roth, M., Wisemberg J., and Vette, J. I., pp. 4-7 to 4-25, in: Development of Improved Models of the Earth's Radiation Environment, Technical Note 1: Model Evaluation, TREND issued at IASB, Printed at MATRA, ESTEC/Contract #8011/88/NL/MAC, 28 June 1989.

"Models of the Trapped Radiation Environment", a series of publications put out initially by the National Aeronautics and Space Administration and later by the National Space Science Data Center (NASA SP-3024, 1966-1971, NSSDC/WDC-A-R&S 72-10, 72-11, 72-13, 74-03, 76-04, 76-06).

Spjeldvik, W.N., and Rothwell, P.L., "The Radiation Belts", pp. 5-31 to 5-39, in: Handbook of Geophysics and the Space Environment, A. S. Jursa (ed.), Air Force Geophysics Laboratory, Air Force Systems Command, United States Air Force, 1985, AFGL-TR-85-0315, ADA167000.